



Performance evaluation of mass transfer correlations in the GFMA process: A review with perspectives to the design



Humberto Estay^{a,*}, Elizabeth Troncoso^b, René Ruby-Figueroa^c, Julio Romero^d

^a Advanced Mining Technology Center (AMTC), University of Chile, Chile

^b Department of Chemistry, Universidad Tecnológica Metropolitana, Las Palmeras 3360, Ñuñoa, Santiago, Chile

^c Programa Institucional de Fomento a la Investigación, Desarrollo e Innovación, Universidad Tecnológica Metropolitana, Ignacio Valdivieso 2409, San Joaquín, Santiago, Chile

^d Laboratory of Membrane Separation Processes (LabProSeM), Department of Chemical Engineering, University of Santiago de Chile (USACH), Chile

ARTICLE INFO

Keywords:

GFMA process
Mass transfer performance
Cyanide recovery
Membrane contactors

ABSTRACT

Gas filled membrane absorption process (GFMA), or hollow fiber gas membranes process (HFGM) can replace two units operations (absorption and stripping) in a unique stage based on membrane contactors. But its application at industrial scale is still emerging: only cases of ammonia removal and concentration have been reported. This advantage has not been enough to scale it up to pilot prototypes for different applications, probably because (i) experimental tests have been carried out with modules that do not exist at industrial scale, and the selection of the mass transfer correlation for different purposes lacks rigour with respect to the original conditions of the correlation, and (ii) industrial modules configurations focused only on gas absorption applications. The first problem limits the experimental results for scientific purposes only, making these results un-reproducible for the design of a pilot or industrial plant. Furthermore, the selection of experimental modules has generally been established to validate an application, limiting the search for an optimal performance. The high quantity of mass transfer correlation also complicates the selection to design or scaling-up purposes. This work includes then a review of the first problem, by conducting an evaluation of mass transfer performance of different membranes modules configuration proposed in literature. The aim is to identify the best experimental configurations for a GFMA process that will lead a further scaling up. This evaluation was carried out using a phenomenological model of GFMA process developed for an application of cyanide recovery in the gold mining industry. The best performance was achieved in membranes modules having cross flow with center baffle and fully baffled.

1. Introduction

1.1. Gas-filled membrane absorption process

The gas-filled membrane absorption process or gas membrane process was developed in 1982 to remove ammonia and iodine and their reabsorption, in sulfuric acid and caustic soda solutions, respectively [1]. This study was expanded in 1985 to strip and absorb different volatile compounds (H_2S , SO_2 , NH_3 , Br_2 , I_2) from aqueous solutions into an absorbent solution [2]. In this process, a hydrophobic hollow fiber membrane contactor (HFMC) is used to separate a feed solution containing a volatile solute (stripping phase) from the receiving phase of the absorption solution. The hydrophobic character of the membrane avoids the penetration of aqueous solutions into the membrane pores, filled with air. Thus, the solute transfer through the membrane is

achieved according to a sequence of steps, as presented in Fig. 1.

The GFMA process has been applied to extract or recover solutes of interest, such as ammonia from wastewater [3–5] and SO_2 from wine [6,7]. Furthermore, the extraction of HCN from different wastewaters has been developed to treat wastewaters [8–13] coupled with coagulation and ion exchange processes. This last application has also been adapted to recover cyanide in gold mining industry [14]. The results of these applications have achieved efficiencies above 90%, using cylindrical modules with parallel flow configuration. A particularity of this application is the use of a reactive absorbent solution which eliminates the resistance to mass transfer presented in step 5 of Fig. 1, because a chemical reaction can be considered fast and performed in the interface of absorbent solution. This result has been demonstrated in a previous work using the Hatta method [14], when the resistance of the absorbed phase is lower than 4% due to the high NaOH

* Correspondence to: Advanced Mining Technology Center (AMTC), University of Chile, Tupper 2007 (AMTC Building), Santiago, Chile.
E-mail address: humberto.estay@amtc.cl (H. Estay).

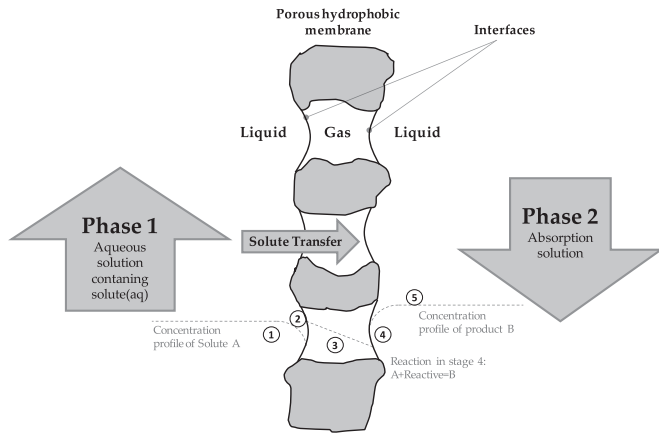
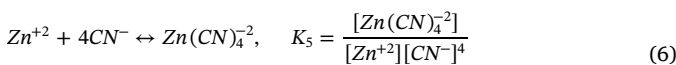
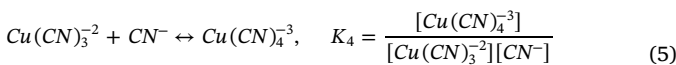
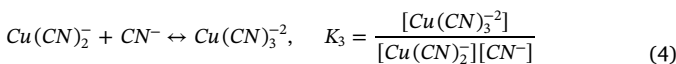
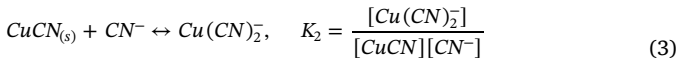
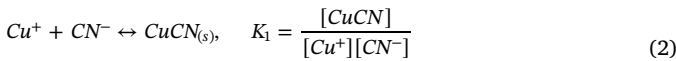
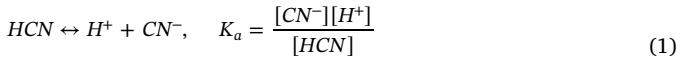


Fig. 1. Scheme of the gas filled membrane absorption process, which shows two gas-liquid interfaces at the pore entrances.

concentration (> 10%wt).

1.2. Phenomenological model of the GFMA process applied to cyanide recovery

A phenomenological model was developed in previous work [14] for the GFMA process to recover cyanide in gold mining. This model can be used to evaluate the performance of the process and also, it can be used for design purposes [15]. The feed solution to be fed into the gas-filled membrane absorption system has to be acidic (pH < 7.0) in order to maximize the content of cyanide as $\text{HCN}_{(\text{aq})}$ in the feed solution. The cyanide-metal complexes contained in the cyanide solution, such as copper and zinc, are dissociated according to the following Eqs. (1)–(6), which include the relationships to describe the chemical equilibrium:



A mass balance for copper, cyanide and zinc can provide a relationship between the concentration of total cyanide, copper, zinc and pH [14]. These relationships are useful to estimate the concentration of metal-cyanides species, as well as the concentration of HCN contained in feed solution as a function of pH. Dissolved HCN is transferred through the membrane pores from feed solution to the absorption phase. This transfer can be described using a model based on a resistances-in-series approach applied on the proximities of the membrane [16]. Thus, the overall HCN transfer through the porous membrane can be described by the following equation:

$$N_{\text{HCN}} = KA\Delta C_{\text{ml}}^{\text{HCN}} \quad (7)$$

where N_{HCN} is the flux of HCN transferred from the cyanidation solution to the absorption phase, K is the overall mass transfer coefficient, A represents the surface area available for mass transfer, and $\Delta C_{\text{ml}}^{\text{HCN}}$ is the logarithmic mean driving force in the cyanidation solution phase

expressed by:

$$\Delta C_{\text{ml}}^{\text{HCN}} = \frac{(C_L^{\text{HCN}} - C_L^{\text{HCN}*})_1 - (C_L^{\text{HCN}} - C_L^{\text{HCN}*})_2}{\ln \left[\frac{(C_L^{\text{HCN}} - C_L^{\text{HCN}*})_1}{(C_L^{\text{HCN}} - C_L^{\text{HCN}*})_2} \right]} \quad (8)$$

$C_L^{\text{HCN}*}$ represents the pseudo-equilibrium concentration of HCN in the cyanidation solution phase, which can be estimated by the following distribution equation:

$$C_L^{\text{HCN}*} = C_L \frac{y_{\text{HCN}}}{m_{\text{HCN}}} \quad (9)$$

In Eq. (9), C_L is the total concentration of the liquid phase, and m_{HCN} is the partition constant (H_{HCN}/P) in mol of HCN in the gas phase per mol of HCN in the liquid phase, which represents the liquid feed-gas equilibrium described by Henry's law for HCN. The overall mass transfer coefficient can be represented as a global resistance, which involves the contribution of individual mass transfer steps. Thus, the overall mass transfer coefficient K can be estimated by means of a resistances-in-series approach applied in the proximities of the membrane according to Eq. (10):

$$\frac{1}{K} = \frac{1}{k_L} + \frac{d_m}{m_{\text{HCN}}k_m d_{\text{ml}}} \quad (10)$$

where k_L is the local mass transfer coefficient in the boundary layer of the cyanide solution phase, and k_m is the local mass transfer coefficient through the gas phase in the membrane pores. A third term on the right side of Eq. (10) referred to the transfer resistance at the receiving phase boundary layer, which can be neglected if the conversion of HCN in cyanide in the receiving solution (Eq. (11)) is considered instantaneous and complete.



The correlation of mass transfer coefficient at the feed boundary layer depends on the circulation configuration of the cyanide solution in the membrane contactor. In this system, the cyanide solution circulates through the shell side in order to maximize the local and overall mass transfer coefficients [4], increasing the transfer area and improving the hydraulic conditions. Therefore, the mass transfer coefficient of the liquid feed boundary layer is estimated using the Basu model [17,18], as shown in Eq. (12).

$$Sh = 17.4(1-\phi) \frac{d_e}{L} Re^{0.6} Sc^{0.33} \quad (12)$$

In Eq. (12), d_e is the equivalent diameter ($4 \times [\text{cross-sectional area of flow}]/[\text{wetted perimeter}]$), L is the length of the membrane contactor, and ϕ is the packing fraction. This correlation was selected for parallel flow configuration according to the module used in the experimental work [14].

Inside the membrane pores, the local mass transfer coefficient for the retained air phase can be described by molecular diffusion.

$$k_m = \frac{D_{\text{HCN-air}} \varepsilon}{\tau e} \quad (13)$$

In Eq. (13), $D_{\text{HCN-air}}$ is the diffusion coefficient of HCN in the air, ε represents the porosity of the fibers, τ is the tortuosity of the fibers and e is the fibers thickness.

1.3. Mass transfer correlations for HFMC

Despite the improvement achieved in this regard, the correct use of the mass transfer correlations is a multi-parametric definition, generating until now an issue for designing and scaling up a membrane contactor process. In this respect, it should be pointed out that the most used mass transfer correlation for lumen side has been developed by Yang and Cussler [19], as shown in the following equation.

Table 1
Mass transfer correlations of the shell side reported in literature.

No.	Correlation	Characteristic length	Module type	Original system	Flow rate	Re	Packing fraction	Refs.
1	$Sh = 1.25 \left(Re \frac{d_e}{L} \right)^{0.95} Sc^{0.33}$	Equivalent diameter ^a	Cylindrical, parallel flow, with no baffles	Stripping of oxygen from water using gas	2–20 cm ³ /s	0–500	0.03–0.26	[19]
2	$Sh = 0.24$	Equivalent diameter ^a	Rectangular cross section, parallel flow, with no baffles	Stripping of oxygen from water using gas	2–20 cm ³ /s	0–0.01	0.4	[19]
3	$Sh = 0.90 Re^{0.40} Sc^{0.33}$	Outer diameter of fibers	Rectangular, cross flow	Stripping of oxygen from water using gas	2–50 cm ³ /s	0–20	0.06	[19]
4	$Sh = 1.38 Re^{0.34} Sc^{0.33}$	Outer diameter of fibers	Rectangular, cross flow	Stripping of oxygen from water using gas	2–50 cm ³ /s	0–20	0.7	[19]
5	$Sh = 8.8 \left(Re \frac{d_e}{L} \right) Sc^{0.33}$	Equivalent diameter ^a	Cylindrical, parallel flow, with no baffles	Proteins solvent extraction	–	–	0.15	[25]
6	$Sh = \beta \left[\frac{d_e(1-\phi)}{L} \right] Re^{0.6} Sc^{0.33}$ $\beta = 6.1$ for hydrophilic membranes $\beta = 5.8$ for hydrophobic membranes	Equivalent diameter ^a	Cylindrical, parallel flow, with no baffles	Solvent extraction	–	0–500 Sc 300–1000	0.04–0.4	[26]
7	$Sh = 17.4 \left[\frac{d_e(1-\phi)}{L} \right] Re^{0.6} Sc^{1/3}$	Equivalent diameter ^a	Cylindrical, parallel flow, with no baffles	Solvent extraction	0–0.6 cm ³ /s	3–60	~ 0.4	[17,18]
8	$Sh = 0.85 \left(\frac{d_s}{d_{out}} \right)^{0.45} \left(\frac{d_s}{L} \right)^{0.57} Re^{0.8} Sc^{1/3}$, laminar flow	Equivalent diameter ^a	Cylindrical, parallel flow, with no baffles	Solvent extraction	–	6–4000	–	[23]
9	$Sh = 0.017 \left(\frac{d_s}{d_{out}} \right) Re^{0.8} Sc^{1/3}$, turbulent flow $Sh = 0.019 Gr^{1.0}$	Equivalent diameter ^a	Cylindrical, parallel flow, with no baffles	Stripping of oxygen from water using nitrogen	146–240 cm ³ /s	Gz < 60	0.7	[28]
10	$Sh = 0.15 Re^{0.8} Sc^{0.33}$, Re > 2.5 $Sh = 0.12 Re^{0.8} Sc^{0.33}$, Re < 2.5	Outer diameter of fibers	Cross flow, cylindrical, helically and rectangular	Stripping of oxygen from water using nitrogen	90–185 cm ³ /s	Re > 2.5 Re < 2.5	–	[28]
11	$Sh = 0.18 Re^{0.86} Sc^{0.33}$	Outer diameter of fibers	Rectangular, cross flow	Stripping of oxygen from water using nitrogen	–	0.1–100	0.36–0.58	[48]
12	$Sh = 0.46 Re^{0.46} Sc^{0.33}$	Outer diameter of fibers	Cylindrical fully baffled	Stripping of oxygen from water using nitrogen	–	0.1–100	0.19	[48]
13	$Sh = 0.49 Re^{0.53} Sc^{0.33}$	Outer diameter of fibers	Cylindrical, axial flow	Stripping of oxygen from water using nitrogen	–	0.03–3	0.19	[21]
14	$Sh = 0.82 Re^{0.49} Sc^{0.33}$	Outer diameter of fibers	Cylindrical, fabric	Stripping of oxygen from water using nitrogen	–	0.1–10	0.13	[21]
15	$Sh = 0.80 Re^{0.46} Sc^{0.33}$	Outer diameter of fibers	Axial, vane	Stripping of oxygen from water using nitrogen	–	0.1–10	0.37	[21]
16	$Sh = (0.53 - 0.58\phi) Re^{0.53} Sc^{0.33}$	Equivalent diameter ^a	Cylindrical, parallel flow, with no baffles	Stripping of oxygen from water using nitrogen	–	–	0.32–0.76	[29]
17	$Sh = 0.24 \left(Re \frac{d_e}{L} \right)^{0.59} Sc^{0.33}$	Equivalent diameter ^a	Fluidized fiber bundle in a submerged jet	Absorption of oxygen in water	–	–	–	[58]
18	$Sh = 1.76 Re^{0.82} Sc^{0.33}$	Equivalent diameter	Cylindrical, cross flow	Solvent extraction	0.05–0.6 m ³ /h	0.02–2	0.49–0.53	[51]
19	$Sh = 8.71 Re^{0.74} Sc^{1/3} \left(\frac{d_e}{L} \right)$	Equivalent diameter ^a	Cylindrical, parallel flow, with no baffles	Solvent extraction	–	0.16–7.3	0.3	[37]

(continued on next page)

Table 1 (continued)

No.	Correlation	Characteristic length	Module type	Original system	Flow rate	Re	Packing fraction	Refs.
20	$k_L = \frac{\Lambda}{(d_{f,L})^b} Q^{c-1} r^{\frac{1}{b}}$ $\Lambda = \frac{a}{d_{out}^{(b-c)}} \left[\frac{d_L}{d_{out}} \right]^{(b-c)} D_L^{(1-c)}$	Outer diameter of fibers	Cylindrical, cross flow	Stripping of oxygen from water using nitrogen	0.11–7.27 m ³ /h	–	–	[56]
<p>a, b and c are constants, f_x is the fractional open area for flow of liquid, ρ_L, μ_L and D_L are density, viscosity and diffusion coefficient of liquid phase.</p>								
21	$Sh = 0.57 Re^{0.31} Sc^{1/3}$	Outer diameter of fibers	Cross flow in a fibers bundle wrapped around a central feeder tube ³¹	Absorption of CO ₂ and/or N ₂ using water	27–2455 cm ³ /min	0–1	–	[50]
22	$Sh = 1.38(-0.07 + 2.35\phi)^{1/3} \left(\frac{1-\phi}{\phi} \right)^{1/3} \left(\frac{2R}{L} \right)^{1/3} Re^{1/3} Sc^{1/3}$	Equivalent diameter ²²	Cylindrical, parallel flow, with no baffles	Theoretical	–	100–250	0.26–0.575	[59]
23	$Sh = 0.09(1-\phi) Re^{(0.8-0.16\phi)} Sc^{0.33}$	Equivalent diameter ²³	Cylindrical, parallel flow, with no baffles	Extraction of ethanol from aqueous solution into n-octanol	–	0–3	0.35–0.79	[30]
24	$Sh = (0.3045\phi^2 - 0.3421\phi + 0.0015) Re^{0.9} Sc^{0.33}$	Equivalent diameter ²⁴	Cylindrical, parallel flow, with no baffles	Oxygen stripping	–	32–1287	0.1–0.7	[31]
25	$Sh = (Sh_1^3 + Sh_2^3 + Sh_3^3)^{1/3}$ $Sh_1 = 3.66 + 1.2(\sqrt{1-\varepsilon})^{0.8}$ $Sh_2 = 1.615(1 + 0.14(\sqrt{1-\varepsilon})^{0.5}) \sqrt{\frac{Re Sc d_e}{L}}$ $Sh_3 = \left(\frac{2}{1+2.2 Sc} \right)^{1/6} \left(\frac{Re Sc d_e}{L} \right)^{1/2}$	Equivalent diameter ²⁵	Cylindrical, parallel flow, with no baffles	–	–	Re < 2300	–	[27]
26	$Sh = 0.56 Re^{0.62} Sc^{0.33}$	Equivalent diameter ²⁶	Cylindrical, cross flow	Solvent extraction of aroma compounds	0.7–400 L/h	3–30	–	[52]
27	$Sh = 0.9 Re^{0.5} Sc^{0.33}$	Outer diameter of fibers	Rectangular, cross flow	CO ₂ absorption from combustion gas	0.5–4 L/h	–	–	[49]
28	$Sh = (0.163 + 0.27\phi) G \phi^{0.6}$	Equivalent diameter ²⁸	Cylindrical, parallel flow, with no baffles	CO ₂ absorption into water	–	178–1194	0.2–0.5	[38]
29	$Sh = 11.7 \left[\frac{1-\phi}{L} \left(\frac{2(1-\phi)}{\phi} \right)^{0.66} Re^{0.66} Sc^{0.33} \right]^{0.78}$	Equivalent diameter ²⁹	Cylindrical, parallel flow, with no baffles	Theoretical	–	< 500	–	[22]
30	$Sh = \frac{1}{(0.86-0.3\phi)^{0.6}} G_z^{(0.3\phi+0.14)}$	Equivalent diameter ³⁰	Cylindrical, parallel flow, with no baffles	Theoretical	–	60–1200	0.1–0.7	[32]
31	$Sh = AR \phi^{0.7} Sc^{0.33}$ $A = (0.1666 - 0.7978\phi + 1.7382\phi^2 - 1.3701\phi^3)$ $SH = 0.1789\phi^{0.86} Re^{0.34} Sc^{0.33}$	Equivalent diameter ³¹	Cylindrical, parallel flow, with no baffles	Stripping of oxygen from water using gas	–	Re > 400	0.293–0.528	[33]
32	$Sh = 2.15 Re^{0.42} Sc^{0.33}$	Equivalent diameter ³²	Cylindrical, cross flow	Stripping of oxygen from water using gas	–	0–20	–	[53]
33	$Sh = 1.89 \beta_z(\phi) (1-\phi)^{1/3} \left[\frac{Re Sc d_{out}}{L} \right]^{1/3}$ <p>Random array: $\beta_z(\phi) = 0.42 + 0.90\phi$ Hexagonal array: $\beta_z(\phi) = 0.51 + 1.44\phi$</p>	Outer diameter of fibers	Cylindrical, parallel flow, with no baffles	Solvent extraction	–	10–80	–	[34]
34	$Sh = 1.45 \left[\frac{Re Sc d_{out}}{L} \right]^{0.33}$	Outer diameter of fibers	Cylindrical, parallel flow, with no baffles	Solvent extraction	–	20–45	0.093–0.402	[35]
35	$Sh = (-0.4575\phi^2 + 0.3993\phi - 0.0475) \times Re^{(4.0108\phi^2 - 4.4296\phi + 1.5585)} Sc^{0.33}$	Equivalent diameter ³⁵	Cylindrical, parallel flow, with no baffles	Osmotic distillation	–	0–0.3	0.306–0.612	[36]
36	$Sh = 6.8695 Re^{0.33344} Sc^{0.33}$	Equivalent diameter ³⁶	Cylindrical, cross flow	Solvent extraction of zinc	0.4–0.8 L/min	0–0.1	–	[54]
37	$Sh = (0.17\epsilon + 0.36) Re^{0.82} Sc^{0.33}$	Equivalent diameter ³⁷	Flat sheet, parallel flow, with no baffles	CO ₂ absorption using NaOH	–	–	–	[24]

(continued on next page)

Table 1 (continued)

No.	Correlation	Characteristic length	Module type	Original system	Flow rate	Re	Packing fraction	Refs.
38	$Sh = 0.055Re^{0.72} Sc^{0.33}$	Equivalent diameter ^c	Cylindrical, cross flow	Solvent extraction	-	0.1–250	0.32–0.45	[55]

^a $d_e = 4 * [\text{cross-sectional area of flow}] / [\text{wetted perimeter}]$.
^b $d_e = 4 * [\text{cross-sectional area of flow}] / [\text{total fiber circumference}]$.
^c $d_e = [d_s^2 - d_{ct}^2 - nd_{out}^2] / [nd_{out}]$, $v_s = [2Q / (\ln(d_s/d_{ct}))] / [\pi L (d_s - d_{ct})]$, $Re = [v_s d_{ct}] / \mu$, where d_s is the internal diameter of shell, d_{ct} is the outer diameter of the central tube, v_s is the velocity in the shell side, Q is the volume flow fed into the shell side.
^d $v_s = Q / A_p$, $A_p = \pi D_{AV} L - (n_p / L_p) d_{out} L$, $D_{AV} = (d_s + d_{ct}) / 2$, where L_p is the number of fibers layers (7 in this case).

$$Sh = 1.64 \left(\frac{d_{in}}{L} Re Sc \right)^{0.33} \tag{14}$$

Where d_{in} is the internal diameter of the fiber. However, for shell side, there are several mass transfer correlations developed in the literature, which can be seen in Table 1, according to the published year. This Table includes the information reported about modules configuration and the range of feed flow treated, Reynolds number and packing fraction. The considerable quantity of correlations developed for hollow fiber contactors applications (gas absorption or solvent extraction) can be an issue for purposes of designing, modeling, and analysis of the performance of the GFMA process. For this reason, Table 2 shows a classification of mass transfer correlations for the shell side according to the module configuration. This table includes cylindrical modules having parallel flow, cross flow, cross flow with center baffle (LiquiCel Extra-Flow configuration), rectangular modules, fully baffled modules, and fabric modules, each one related to its mass transfer correlation obtained in the specific work cited. This classification is a useful methodology to select the mass transfer correlation adjusted to an application. According to our previous work, around 99% of the mass transfer resistance in the GFMA process applied to recover cyanide belongs to the aqueous phase circulating in the shell side [14]. For the above reason, it is relevant to define the correct mass transfer correlation on the shell side and the impact on the performance results of GFMA process.

A recent work proposes an interesting module configuration with a new fiber arrangement [20]. Nevertheless, the characterization of a mass transport on the shell side through a correlation of the transfer coefficient was not reported.

In this framework, the aim of this work is the performance assessment of the GFMA process, in a cyanide recovery operation, using different membrane modules configuration in order to establish the best HFMC to use at pilot or industrial scale. Furthermore, a critical evaluation of the different mass transfer correlations for the typical modules used at laboratory scale (cylindrical with parallel flow) is carried out to demonstrate the high variability of the results obtained for each one and the relevance of the based-conditions for each correlation.

2. Methodology

2.1. Re-validation of the mass transfer correlation on the shell side

The phenomenological model of the GFMA process to recover cyanide, developed in a previous work [14], defined the Basu correlation [17] for the mass transfer on the shell side. In this part, a comparison of mass transfer coefficients obtained by each mass transfer correlation has been carried out on the shell side for cylindrical modules with parallel flow. For this purpose, the simulated operational conditions were the same as those used in the previous work [14], where an experimental cylindrical module with parallel flow was used. Table 3 shows these experimental conditions, which were used to validate the phenomenological model in the previous work and re-validate the mass transfer correlation on the shell side for a cylindrical module with parallel flow for this work, as reported in Table 3. Thus, the overall mass transfer coefficient was estimated using Eqs. (10), (12) and (13), changing the Eq. (12) according to the mass transfer correlation used from Table 2 for cylindrical modules with parallel flow. In this way, three mass transfer correlations with the best adjustment with respect to the overall mass transfer coefficient were selected from previous work. They were also tested in the phenomenological model with the goal of comparing the cyanide recovery results with the experimental results previously reported in literature [14].

2.2. Performance assessment of different membrane configurations

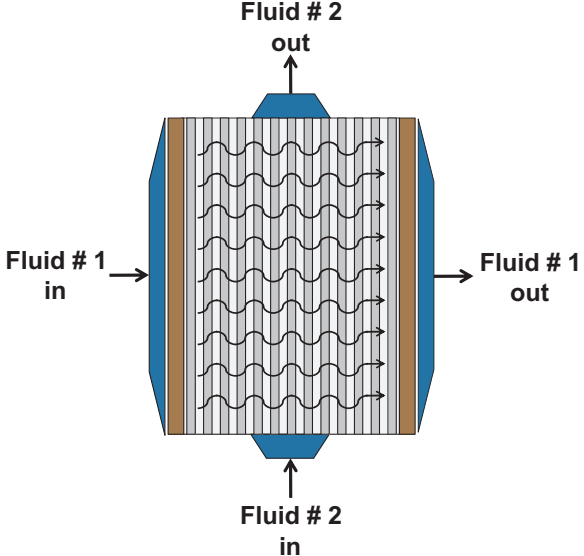
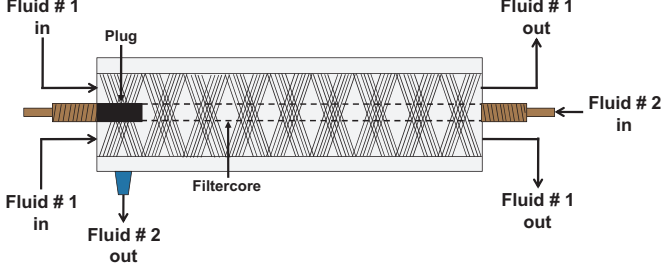
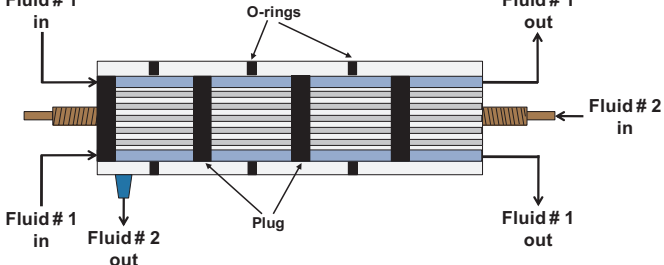
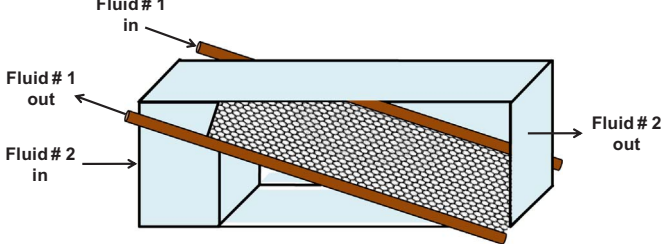
Table 2 shows 8 different modules configurations with respect to the

Table 2
Classification of mass transfer correlations of the shell side according to the module configuration.

Correlation	Correlation	Configuration	Refs.
Yang and Cussler [19]	$Sh = 1.25 \left(Re \frac{d_e}{L} \right)^{0.93} Sc^{0.33}$	<p style="text-align: center;">Cylindrical module, parallel flow, no baffles</p> <p style="text-align: center;">Hollow fiber membranes</p>	[19]
Dahuron and Cussler [25]	$Sh = 8.8 \left(Re \frac{d_e}{L} \right) Sc^{0.33}$		[25]
Prasad and Sirkar [26]	$Sh = \beta \left[\frac{d_e(1-\phi)}{L} \right] Re^{0.6} Sc^{0.33}$ $\beta = 6.1$ for hydrophilic membranes $\beta = 5.8$ for hydrophobic membranes		[26]
Basu et al. [17]	$Sh = 17.4 \left[\frac{d_e(1-\phi)}{L} \right] Re^{0.6} Sc^{1/3}$		[17,18]
Wickramasinghe et al. [28]	$Sh = 0.019 Gr^{1.0}$		[28]
Costello et al. [29]	$Sh = (0.53 - 0.58\phi) Re^{0.53} Sc^{0.33}$		[29]
Viegas et al. [37]	$Sh = 8.71 Re^{0.74} Sc^{1/3} \left(\frac{d_e}{L} \right)$		[37]
Bao et al. [59]	$Sh = 1.38(-0.07 + 2.35\phi) \left(\frac{1-\phi}{\phi} \right)^{1/3} \left(\frac{2R}{L} \right)^{1/3} Re^{1/3} Sc^{1/3}$		[59]
Gawronski and Wrzesinska [30]	$Sh = 0.09(1 - \phi) Re^{(0.8-0.16\phi)} Sc^{0.33}$		[30]
Wu and Chen [31]	$Sh = (0.3045\varphi^2 - 0.3421\varphi + 0.0015) Re^{0.9} Sc^{0.33}$		[31]
Lipnizki and Field [27]	$Sh = (Sh_1^3 + Sh_2^3 + Sh_3^3)^{1/3}$ $Sh_1 = 3.66 + 1.2(\sqrt{1-\varepsilon})^{-0.8}$ $Sh_2 = 1.615(1 + 0.14(\sqrt{1-\varepsilon})^{-0.5}) \sqrt{\frac{Re Sc d_e}{L}}$ $Sh_3 = \left(\frac{2}{1+22 Sc} \right)^{1/6} \left(\frac{Re Sc d_e}{L} \right)^{1/2}$		[27]
Zheng et al. [38]	$Sh = (0.163 + 0.27\phi) Gz^{0.6}$		[38]
Koo and Sangani [22]	$Sh = 11.7 \left[\frac{1-\phi}{L} \left(\frac{2(1-\phi)}{\phi} \right)^{0.66} Re^{0.66} Sc^{0.33} \right]^{0.78}$		[22]
Zheng et al. [32]	$Sh = \frac{1}{(0.86-0.3\phi)\phi_0} Gz^{(0.3\phi_0+0.14)}$		[32]
Kartohardjono et al. [33]	$Sh = A Re^{0.7} Sc^{0.33}$ $A = (0.1666 - 0.7978\varphi + 1.7382\varphi^2 - 1.3701\varphi^3)$ $Sh = 0.1789\varphi^{-0.86} Re^{0.34} Sc^{0.33}$		[33]
Asimakopoulou and Karabelas [34]	$Sh = 1.89\beta_z(\phi)(1-\phi)^{1/3} \left[Re Sc \frac{d_{out}}{L} \right]^{1/3}$ Random array: $\beta_z(\phi) = 0.42 + 0.90\phi$ Hexagonal array: $\beta_z(\phi) = 0.51 + 1.44\phi$		[34]
Asimakopoulou and Karabelas [35]	$Sh = 1.45 \left[Re Sc \frac{d_{out}}{L} \right]^{0.33}$		[35]
Thanedgunbaworn et al. [36]	$Sh = (-0.4575\phi^2 + 0.3993\phi - 0.0475) \times Re^{(4.0108\phi^2 - 4.4296\phi + 1.5585)} Sc^{0.33}$		[36]
Zhang et al. [24] ^a	$Sh = (0.17\varepsilon + 0.36) Re^{0.82} Sc^{0.33}$		[24]
Takeushi et al. [23]	$Sh = 0.85 \left(\frac{d_s}{d_{out}} \right)^{0.45} \left(\frac{d_e}{L} \right)^{1/4} Re^{1/3} Sc^{1/3}$, laminar flow $Sh = 0.017 \left(\frac{d_s}{d_{out}} \right)^{0.57} Re^{0.8} Sc^{1/3}$, turbulent flow	Applied with one fiber only. [23]	
Yang-Cussler, Rectangular	$Sh = 0.24$	[19]	

(continued on next page)

Table 2 (continued)

Correlation	Correlation	Configuration	Refs.
Yang-Cussler, Cross Flow 72 fibers	$Sh = 0.90Re^{0.40} Sc^{0.33}$	<p style="text-align: center;">Rectangular modules, cross flow</p> 	[19]
Yang-Cussler, Cross Flow, 750 fibers	$Sh = 1.38Re^{0.34} Sc^{0.33}$		
Wickramasinghe, handmade parallel	$Sh = 0.49Re^{0.53} Sc^{0.33}$	<p style="text-align: center;">Cylindrical handmade module, parallel flow</p> 	[21]
Wickramasinghe, handmade parallel baffled	$Sh = 0.82Re^{0.49} Sc^{0.33}$	<p style="text-align: center;">Cylindrical handmade module, parallel flow, with baffles</p> 	[21]
Wickramasinghe, handmade rectangular	$Sh = 0.80Re^{0.46} Sc^{0.33}$	<p style="text-align: center;">Rectangular handmade module, cross flow</p> 	[21]

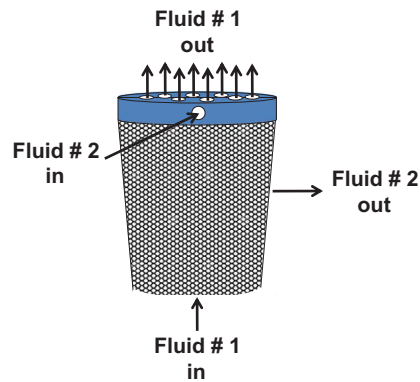
(continued on next page)

Table 2 (continued)

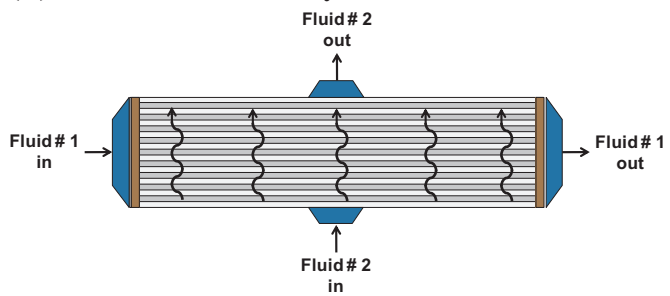
Correlation	Correlation	Configuration	Refs.
-------------	-------------	---------------	-------

Wickramasinghe, Cross Flow '92
 $Sh = 0.15Re^{0.8} Sc^{0.33}, Re > 2.5$
 $Sh = 0.12Re^{0.8} Sc^{0.33}, Re < 2.5$

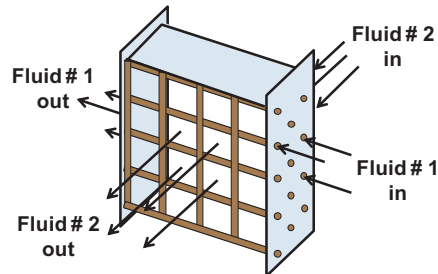
[28]



(A) Flow across a helically wound bundle.



(B) Flow across a cylindrical bundle.

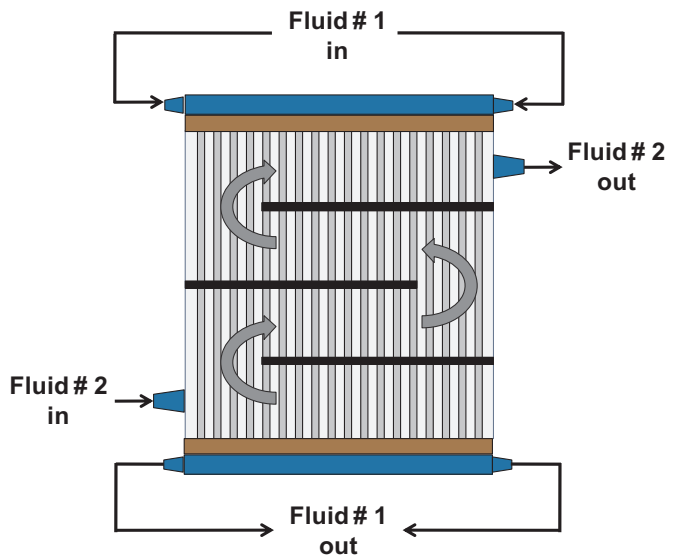


(C) Flow across a rectangular bundle.

Wang-Cussler, Cross Flow
 $Sh = 0.18Re^{0.86} Sc^{0.33}$

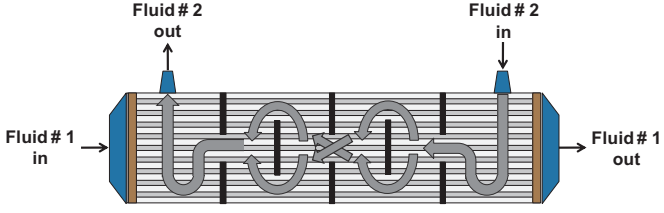
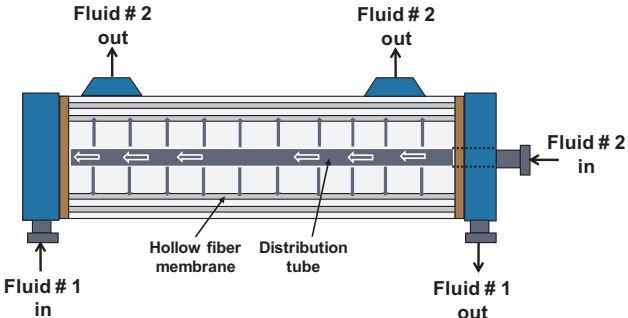
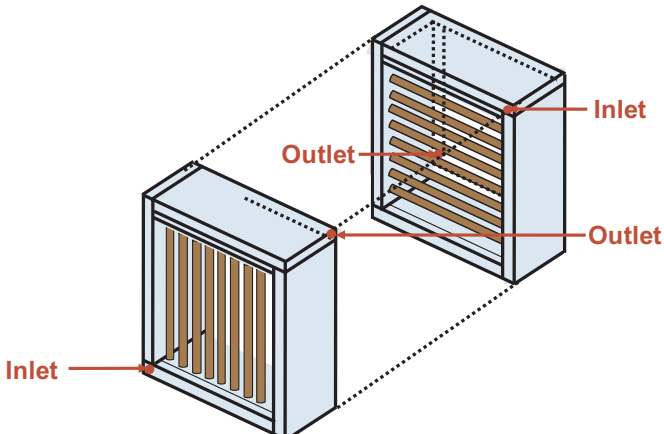
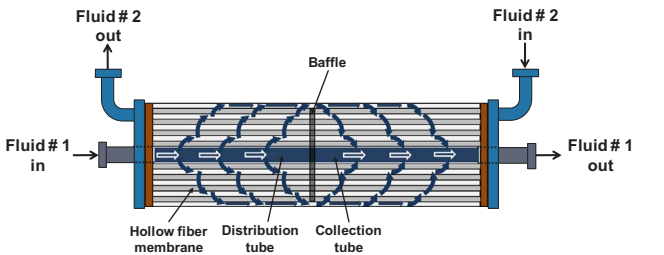
[48]

Rectangular module, cross flow, with baffles



(continued on next page)

Table 2 (continued)

Correlation	Correlation	Configuration	Refs.
Wang-Cussler, Fully Baffled	$Sh = 0.46Re^{0.46} Sc^{0.33}$	Cylindrical module, parallel flow, fully baffles 	[48]
Bhaumik et al., Cross flow	$Sh = 0.57Re^{0.31} Sc^{1/3}$	Cylindrical module, cross flow with fibers bundle wrapped around a central feeder tube 	[50]
Feron, Cross Flow	$Sh = 0.9Re^{0.5} Sc^{0.33}$	Rectangular module, cross flow 	[49]
Schoner, LiquiCel 2.5 × 8	$Sh = 1.76Re^{0.82} Sc^{0.33}$	Cylindrical module, cross flow with center baffle (LiquiCel module) 	[51]
Baudot, LiquiCel 2.5 × 8	$Sh = 0.56Re^{0.62} Sc^{0.33}$		[52]
Zheng, LiquiCel 2.5 × 8	$Sh = 2.15Re^{0.42} Sc^{0.33}$		[53]
Fouad, LiquiCel 2.5 × 8	$Sh = 6.8695Re^{0.33344} Sc^{0.33}$		[54]
Shen, LiquiCel 2.5 × 8	$Sh = 0.055Re^{0.72} Sc^{0.33}$		[55]
Sengupta, LiquiCel	$k_L = \frac{\Lambda}{(\pi f_x L)^b} Q^{b \frac{1}{b}}$ $\Lambda = \frac{a}{d_{out}^{(1-b)}} \left[\frac{\rho L}{\mu L} \right]^{(b-c)} D_L^{(1-c)}$		[56]

^a This correlation was estimated from an experimental flat sheet module tube applied in cylindrical modules.

conventional cylindrical modules with parallel flow and no baffles (experimental module), namely: (i) cylindrical module with parallel flow and fully baffled; (ii) rectangular module with parallel flow and no baffles; (iii) cylindrical module with cross flow; (iv) rectangular module with cross flow and no baffles; (v) rectangular module with cross flow and baffles; (vi) cylindrical handmade module with parallel flow; (vii) rectangular handmade module with cross flow; and (viii) cylindrical module with cross flow and center baffle (LiquiCel module). Table 4

summarizes the characteristics of the different modules simulated, although the information regarding the three handmade modules developed by Wickramasinghe and collaborators (1993) [21] was not enough to use it in the phenomenological model. Simulations were performed using the same feed flows and operational conditions tested in the experimental work (Table 3), despite the capacities reported for different modules. This assumption will be discussed in the results section. Also, the mass transfer correlations included in the

Table 3
Operational conditions and membrane contactor parameters used in the previous work [14].

Description	Value	Unit
Feed tank volume	0.5	L
Absorption tank volume	0.5	L
Feed cyanide solution flow	0.5; 1.0; 2.0	L min ⁻¹
Feed-Absorption flow ratio	1	L L ⁻¹
pH of cyanide solution	5	–
Total cyanide concentration	~ 2000	mg L ⁻¹
Copper concentration	100	mg L ⁻¹
Zinc concentration	500	mg L ⁻¹
Temperature	15	°C
Membrane material	polypropylene	–
Number of fibers	7400	–
Surface contact area	0.58	m ²
Fiber outside diameter	330	μm
Fiber inside diameter	220	μm
Shell inside diameter	0.043	m
Membrane contactor length	0.12	m

phenomenological model for each module responded to the specific correlation determined by the author who proposed the module configuration (Table 2).

This part involves the analysis of different correlations to estimate the mass transfer coefficient on the shell side of LiquiCel modules.

2.3. Statistical analysis

Data obtained as described in the Sections 2.1 and 2.2 were evaluated and compared using a statistical method. The agreement assessment of the model was carried out by using the root mean square error (RMSE) and the mean absolute error (MAE). Moreover, an ANOVA regression analysis ($\alpha = 0.05$) was performed in order to evaluate the degree of fitting for each model. On the other hand, a model validation routine was carried out, for each model, using residual analysis. Adapted Kolmogorov–Smirnov and Shapiro–Wilk tests were used for this purpose, this means, corroborating that the associated residual has a normal distribution at a 95% of a confidential level.

3. Results and discussion

3.1. Re-validation of the mass transfer correlation on the shell side

The overall mass transfer coefficient was estimated using each mass transfer correlation on the shell side for cylindrical module with parallel flow, as reported in Table 2. Fig. 2 shows the values of the overall mass transfer coefficient in a wide range: between 10^{-5} and 10^{-7} m/s, estimated from different mass transfer correlations, demonstrating the high variability of mass transfer coefficient values obtained from those. Also, Fig. 2 does not show the results from correlations of Koo and Sangani [22], Takeushi et al. [23], and Zhang et al. [24], because they are out of scale in the graph. The estimating values of the overall mass transfer coefficient are higher than 10^{-4} m/s to the operational conditions simulated, having a difference between one and three orders of magnitude with respect to the rest of mass transfer correlations shown in Table 2. The common factor between these three correlations was the methodology used to determine them. Koo and Sangani [22] obtained a correlation using a theoretical method for laminar flow, which overestimates the mass transfer coefficient value due to the packing fraction dependence included in the equation. Hence, Sh numbers were obtained with two orders of magnitude higher than these correlations. Takeushi and collaborators [23] determined a correlation based on a single-fiber module, therefore the hydrodynamic module on the shell side is different in relation to the packed-fiber modules. This correlation also overestimates the mass transfer coefficient, because of the higher value of the d_s/d_{out} ratio. Finally, Zhang et al. [24] carried out a study

in a flat sheet module, obtaining an experimental correlation that depends on the porosity of the fibers.

There are several mass transfer correlations evaluated in this study, providing different results than those obtained from the mass transfer coefficient estimated in the previous one. Yet, the main reason for the worst adjustment for these mass transfer correlations is the difference between the operational conditions assessed by these works in relation to the previous study [14]. In this framework, some correlations were obtained using packing fractions lower than those used for the GFMA process, such as Yang and Cussler ($\phi = 0.03$ – 0.26) [19], Dahuron and Cussler ($\phi = 0.15$) [25], and Prasad and Sirkar ($\phi = 0.04$ – 0.4) [26]. The effect and importance of the packing fraction on the mass transfer coefficient value of the shell side have been studied and discussed by different authors, saying for example, that “considerable room for bypassing and channeling” is caused when packing fraction is lower than 0.2 [17,19,27]. Thus, the shell-side mass transfer behavior will vary widely from module to module, so there will be much less of an extent of channeling in a densely packed module, resulting in a much higher transfer coefficient. On the other hand, there are studies which report tests using high values of packing fraction, such as Wickramasinghe et al. ($\phi = 0.7$) [28], Costello et al. ($\phi = 0.32$ – 0.76) [29], and Gawronski and Wrzesinska ($\phi = 0.35$ – 0.79) [30]. These correlations do not fit with the mass transfer coefficient values from the previous work, even demonstrating worse results when packing fraction had increased in a range between 0.3 and 0.76 [29]. Therefore, the high packing fraction can promote dead zones due to touching fibers, reducing the available membrane area for mass transfer.

Another relevant parameter capable of affecting the mass transfer coefficient is the Sc number. Some studies [19] have been performed by flowing the gas phase through the shell side. They have determined a Sc value one or two magnitude orders lower than the Sc number assessed in the GFMA process when an aqueous solution is circulating for cylindrical modules with parallel flow. In this case, the results obtained from the correlation by Yang and Cussler [19], applied for the GFMA process, can be explained by the Sc value observed on the shell side.

Certainly, the packing fraction of the module and the physical properties of the phase circulating in the shell side (related to the Sc number) seem relevant parameters that determine the performance of the GFMA process, although the Re number value on the shell side is determinant in the mass transfer coefficient.

The operational conditions (Re values between 4 and 17) determined by previous studies -which determined the correlations in Fig. 2 – explain the differences in the overall mass transfer values estimated in Fig. 2. There are mass transfer correlations obtained for high values of Re number (30–1300 [31]; 10–3200 [27]; 70–1200 [32]; 100–7000 [33]), slightly high values of Re number (10–80 [34]; 20–45 [35]; 10–143 [36]) and Re values lower than those tested in the previous work (< 3 [30]).

Thus, the estimation of the overall mass transfer coefficient shown in Fig. 2 indicates a better agreement with respect to the values obtained in the previous work [14] for the correlations by Basu et al. [17], Viegas et al. [37], and Zheng et al. [38]. These three correlations were obtained for packing fractions values similar to the experimental module ($\phi = 0.37$), and circulating a liquid phase in the shell side, organic [17,37] or aqueous [38], which implies that there were around 700 Sc numbers (the experimental Sc number was of 747). However, the Re numbers on the shell side reported by these authors are different compared with the Re numbers used in the experimental tests performed in previous studies ($Re = 4$ – 17) [14]. Here, Viegas et al. [37] carried out their work in a range of Re numbers of 0.16–7.3, increasing the difference in the overall mass transfer coefficient estimated for high flows, and Zheng et al. [38] used Re numbers between 170 and 1200 approximately. These results indicate that the packing fraction and the Sc number largely affect the mass transfer coefficient. However, there are several mass transfer correlations which differ only in the Re number used [27,31–36]. Regardless of the difference between these

Table 4
Membrane contactors characteristics for the different modules configuration described in Table 2.

Description	Rectangular module, parallel flow [19]	Rectangular module, cross flow 1 [19]	Rectangular module, cross flow 2 [19]	Different modules, cross flow ^b [28]	Rectangular module, cross flow ^c [48]	Cylindrical module, parallel flow, fully baffled [48]	Cylindrical module, cross flow, fibers bundle wrapped around a feeder tube [50]	Cylindrical module with center baffle (LiquiCel 2.5 × 8) [51]	Rectangular module, cross flow [49]	Unit
Flow capacity reported	0.12–3.0	0.12–3.0	0.12–3.0	5.4–11.1	NR ^d	NR	0.1–2.45	1.7–11.7	0.008–0.07	L min ⁻¹
Membrane material	polypropylene	polypropylene	polypropylene	polypropylene	polypropylene	polypropylene	polypropylene	polypropylene	polypropylene	–
Number of fibers	2100	72	750	32,000	3245	256	1050	9950	700	–
Surface contact area	0.6	0.01054	0.1098	3.2	0.221	0.0639	0.2276	1.4	0.27	m ^b
Fiber outer diameter	439.5	466	466	245	300	460	300	300	1000	µm
Fiber inside diameter	413	439.5	439.5	220	270	430	240	220	600	µm
Shell inside diameter ^a	$H \times A = 0.012 \times 0.01$	$H \times A = 0.1 \times 0.01$	$H \times A = 0.1 \times 0.01$	$H \times A = 0.13 \times 0.13$	$H \times A = 0.075 \times 0.014$	0.014	0.027	0.056	$H \times A = 0.05 \times 0.05$	m
Center tube diameter	–	–	–	–	–	–	0.022	0.0222	–	m
Packing fraction	0.4	0.06	0.7	0.09	0.37	0.19	–	0.53	0.22	–
Overall mass transfer coefficient ^e	1.68×10^{-6}	$(4.33-7.54) \times 10^{-5}$	$(6.16-9.87) \times 10^{-5}$	$(0.72-2.87) \times 10^{-6}$	$(2.47-8.15) \times 10^{-5}$	$(0.66-1.25) \times 10^{-4}$	$(1.79-2.75) \times 10^{-5}$	$(2.36-7.36) \times 10^{-5}$	$(2.11-4.22) \times 10^{-5}$	m/s
Membrane fiber length	0.22	0.1	0.1	0.13	0.075	0.186	0.23	0.15	0.5	m
Author	Yang-Cussler	Yang-Cussler	Yang-Cussler	Wickramasinghe et al. [28]	Wang-Cussler	Wang-Cussler	Bhaumik et al.	LiquiCel	Feron et al.	–

^a For rectangular modules is used height(H) and width(W) dimensions.
^b The correlation obtained for these modules was similar, hence the simulations have been carried out using the data from rectangular module.
^c The correlation obtained for these modules was similar for cases with and with no baffles, hence the simulations have been carried out using the data from rectangular modules with no baffles.
^d NR: Not reported.
^e Estimated by phenomenological model, using operational conditions of Table 3 and module characteristics reported here.

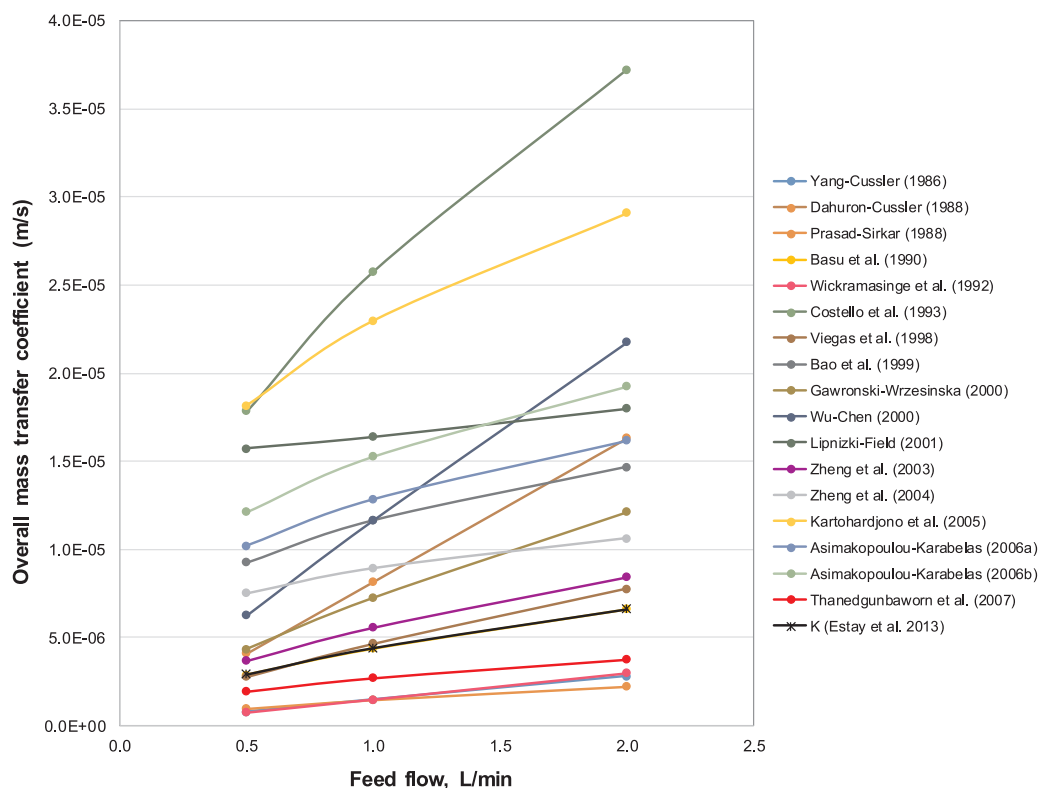


Fig. 2. Results of overall mass transfer coefficient for each mass transfer correlation of the shell side in cylindrical modules with parallel flow.

mass transfer correlations is less than one order of magnitude, a difference for an estimation of the mass transfer coefficient value is expected, which might trigger a huge difference for purposes of design and performance assessment. Therefore, the selection and use of mass transfer correlations for design purposes has to take into account the type of module used, the phase of the fluid circulating in both sides of the membrane (lumen and shell), the valid ranges for packing fraction, and Re numbers in order to delimit the wide range of results by the different mass transfer correlations. Also, it is highly recommended to analyze a set of “candidate” correlations and compare it with experimental results or modeling predictions, as well as a model validation by residuals analysis. It is also relevant to mention that the choice of mass transfer correlations for studies running under specific operational conditions is the fair selection of mass transfer correlation. This means to consider an adequate method for supporting the use of correlations, in order to avoid poorly fitted or over fitted models [39–45].

The three mass transfer correlations that estimate values of mass transfer coefficients closer to the estimated ones in the previous studies have been selected to test the phenomenological model in order to fit with the experimental results. These results are shown in Figs. 3–5 for different evaluated feed flows.

Table 5 shows a comparison of the experimental cyanide recovery in relation to the calculated recovery obtained for each model. Furthermore, the statistical degree of fitting for the selected models is shown in Table 5. Model selection can be performed on the base of highest R-squared and F-ratio, and the minimum RSME and MAE, respectively. However, it should be considered that the model must be validated in terms of residual analysis, because the parameters already mentioned measure the fraction of the total variability in the cyanide recovery that is accounted by the model only [46]. In this case, according to the data shown in Table 5, the selected models showed an R-squared higher than 97.2418%, higher values of F-ratio, and lower values of RMSE and MAE for all the velocities tested. In the residuals analysis the random behavior of the residual needs to be checked, which is an indication that the model does not present autocorrelation [47]. The analysis then

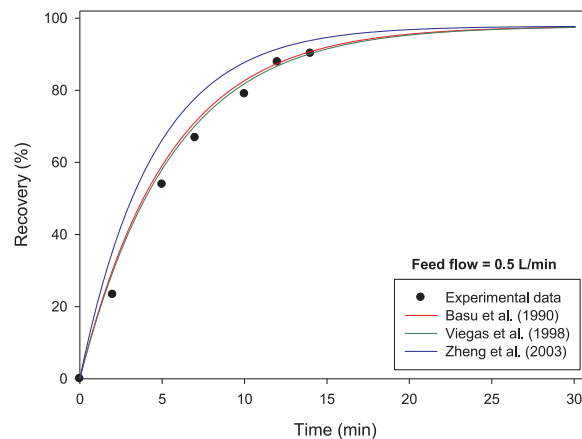


Fig. 3. Results of cyanide recovery using different mass transfer correlations performed by the phenomenological model of the GFMA process and the previous experimental work [14], for a feed flow of 0.5 L/min.

shows a normal distribution of the residuals with p-values higher than 0.05 (Modified Kolmogorov-Smirnov and Shapiro-Wilks) for all the velocities studied. Despite the fact all the models have shown higher goodness-of-fit, some differences were appreciated among them. In particular, the model reported by Basu et al. [17] was the only one which correlates better the data for a velocity of 2.0 L/min. On the other hand, for a velocity of 1.0 L/min, the model showing the best goodness-of-fit was the one reported by Zheng et al. [38]. In the case of data at 0.5 L/min, the model reported by Viegas et al. [37] was the model showing the best goodness-of-fit.

3.2. Performance assessment of different membrane configurations

The phenomenological model developed previously [14] has been modified according to the hollow fiber membrane contactor used, as

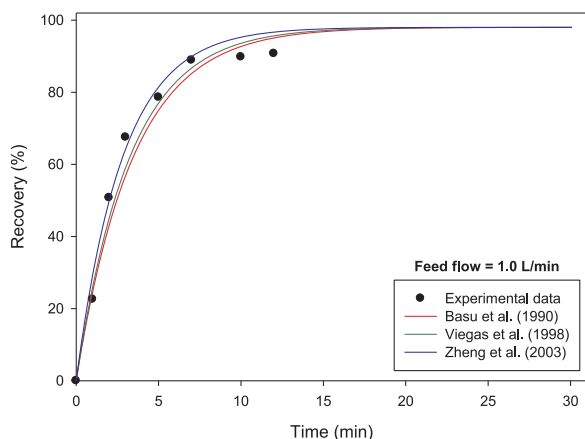


Fig. 4. Results of cyanide recovery using different mass transfer correlations performed by the phenomenological model of the GFMA process and the previous experimental work [14], for a feed flow of 1.0 L/min.

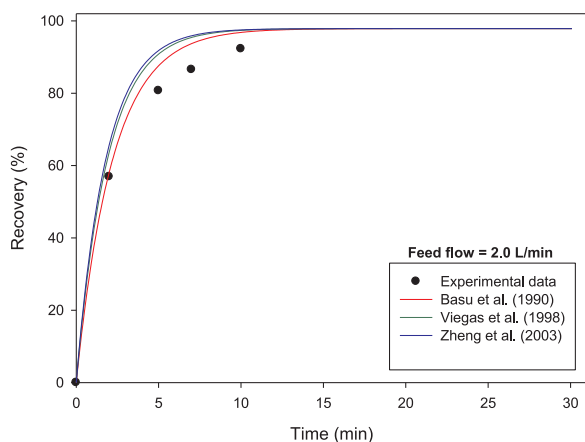


Fig. 5. Results of cyanide recovery using different mass transfer correlations performed by the phenomenological model of the GFMA process and the previous experimental work [14], for a feed flow of 2.0 L/min.

shown in Tables 2 and 4. Simulation results of cyanide recovery are shown in Figs. 6–8, with feed flows ranging from 0.5 to 2.0 L/min. For each flow simulated, the LiquiCel 2.5 × 8 module obtained the best cyanide recoveries. Instead, the rectangular configurations of Yang and Cussler [19], with parallel and cross flow (72 fibers), presented the worst results. Also, the modules with cross flow from Wang and Cussler [48], Yang and Cussler (750 fibers) [19], and Feron [49] had lower cyanide recovery results, but closer to the LiquiCel module. Furthermore, the fully baffled module from Wang and Cussler [48], the rectangular module with cross flow from Wickramasinghe et al. [28], and the cylindrical module with cross flow from Bhaumik et al. [50],

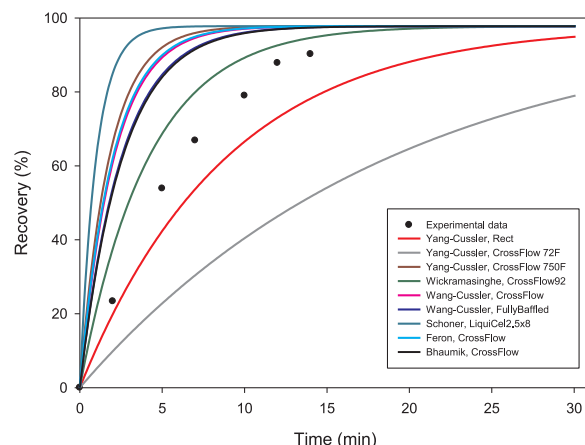


Fig. 6. Results of cyanide recovery of mass transfer correlations from different modules configurations (Table 4) used by the phenomenological model of the GFMA process, for feed flow of 0.5 L/min.

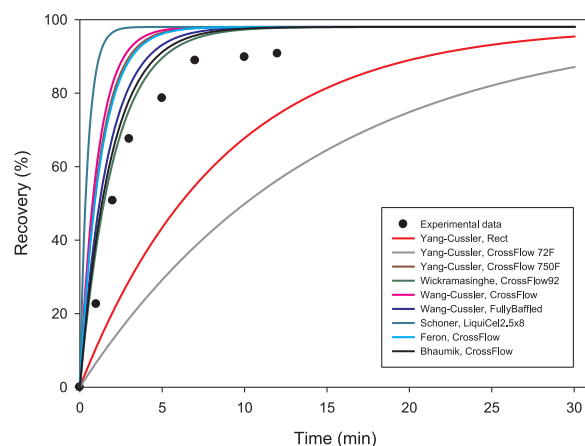


Fig. 7. Results of cyanide recovery of mass transfer correlations from different modules configurations (Table 4) used by the phenomenological model of the GFMA process, for feed flow of 1.0 L/min.

achieved cyanide recoveries slightly higher than the experimental results from the cylindrical module with parallel flow. In general, the results show similar tendencies for each module with respect to the feed flow variations, except for the cross flow modules from Feron [49] and Wang and Cussler [48], which increased faster than the other modules when feed flow increased as well. However, when mass transfer coefficients values were reviewed (Table 4), it was possible to assert that the module with the best performance was the fully baffled module from Wang and Cussler [48], reaching overall mass transfer coefficient values ranging from 0.66 to 1.25×10^{-4} m/s, despite its lower cyanide

Table 5
Statistical analysis of the degree of fitting on the rejection for the studied models.

Correlation	Experimental condition (feed flow, L/min)	MAE	RMSE	R-squared ^a	F-ratio	MK-S test	S-W test
Basu et al. [17]	0.5	2.47629	3,960343	99.1613	710.36	≥ 0.10	0.362586
	1	4.48357	5,356305	97.2418	247.79	≥ 0.10	0.643787
	2	1.43209	4,921311	99.7358	1510.84	≥ 0.10	0.335832
Viegas et al. [37]	0.5	2.23645	3,330165	99.3055	858.90	≥ 0.10	0.593595
	1	3.9029	4,132849	97.8259	315.98	≥ 0.10	0.64048
	2	1.53929	7,119846	99.5897	971.99	≥ 0.10	0.618985
Zheng et al. [38]	0.5	4.17598	8,664703	97.6096	246.00	≥ 0.10	0.236759
	1	2.6716	3,452896	98.7869	571.02	≥ 0.10	0.627239
	2	1.9444	7,936556	99.3646	626.50	≥ 0.10	0.431452

^a Adjusted to degree of freedom.

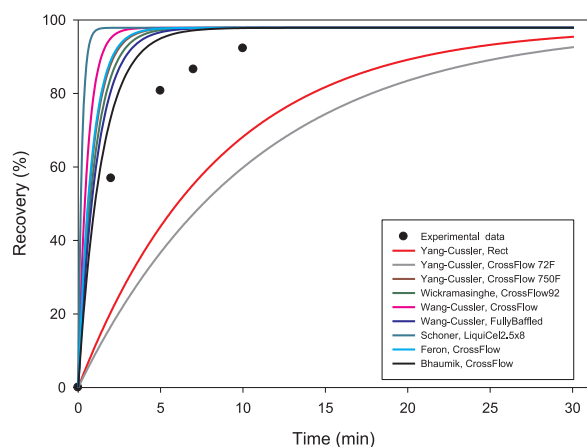


Fig. 8. Results of cyanide recovery of mass transfer correlations from different modules configurations (Table 4) used by the phenomenological model of the GFMA process, for feed flow of 2.0 L/min.

recovery results than others configurations. This result is explained by the mass transfer area available in this module: only 0.0639 m^2 , the lowest of all modules. On the other hand, the worst module performance was obtained by the rectangular module with parallel flow from Yang and Cussler [19] and the cross flow modules from the results reported by Wickramasinghe and collaborators [28], reaching mass transfer coefficients values lower than $3.0 \times 10^{-6} \text{ m/s}$. The other configurations had mass transfer coefficients values ranging from 1.79 to $9.9 \times 10^{-5} \text{ m/s}$, where the modules of LiquiCel and cross flow used by Wang and Cussler [48] presented a higher effect of the flow rate on the mass transfer coefficient in the shell side. This fact is highly important for modules where the reported capacity is higher than the feed flow simulated. E.g., the LiquiCel module can process up to 11.7 L/min, and the maximum simulated feed flow was 2.0 L/min. Therefore, the flow velocity in the shell side could be much greater, increasing the overall mass transfer coefficient ($3.13 \times 10^{-4} \text{ m/s}$, according to a simulation for this feed flow) over the values of the other modules reported in Table 4. Hence, the cross flow with center baffle module from LiquiCel can achieve the best performance with respect to the others modules configuration, operating at the maximum tolerable feed flow. However, the increase in the pressure drop must be taken into account when the module is operated at maximum tolerable feed flow condition (0.1 bar for the LiquiCel 2.5 × 8 module at maximum feed flow [51]). With this in mind, the mass transfer coefficient values of the fully baffled module from Wang and Cussler [48] obtained in the simulations could be overestimated, due to the high velocity reached in the shell side promoted by a feed flow higher than the tolerable capacity of the module. Unfortunately, the capacity of this module was not reported by the authors, although the experimental conditions were adjusted to get Re values from 1 to 100. Thus, the maximum tolerable feed flow is estimated for the maximum Re number, given a result close to 1.7 L/min. Yet, the value of the overall mass transfer coefficient was $1.1 \times 10^{-4} \text{ m/s}$ under this condition. Even though this value is lower than the one obtained for the maximum flow of LiquiCel module, when a comparison at the same feed flow is performed, the fully baffled module does achieve better performance. Nevertheless, the maximum pressure drop reached by the fully baffled module at the maximum feed flow has not been reported. This information is critical to select a module for scaling up or for industrial application purposes. In this regard, the rectangular module with cross flow by Feron [49] obtained good cyanide recovery results, although the tolerable reported feed flows are significantly lower than the simulated feed flows, so that the pressure drop expected in this module could be very high. On the other hand, the simulated feed flows for the rectangular module with cross flow from Wickramasinghe and collaborators [28] are lower than the capacity reported by the authors. A simulation of the maximum flow for

this module reached an overall mass transfer coefficient value equal to $1.6 \times 10^{-5} \text{ m/s}$, which is lower than the fully baffled and LiquiCel modules. Furthermore, the results simulated for feed flows of 0.5 and 1.0 L/min in the LiquiCel modules must be validated with further experimental work, due to the possible “dead zones” generated at low feed flows. The occurrence of “dead zones” can decrease the mass transfer coefficient, affecting the performance of the process. The phenomenological model does not include this phenomenon, so the results obtained confirm the good performance achieved by the Extra-Flow modules from LiquiCel. Here, the center baffle promotes a cross flow which increases the turbulence in the shell side, although the fully baffled module designed by Wang and Cussler [48] presents interesting performance results for a GFMA process application. However, there are no reports of the pressure drop data for these types of modules, and its industrial fabrication is not available (different types of modules having higher capacities). Further studies, or directly an industrial fabrication, could be interesting to expand the offer of hollow fiber membrane contactors for GFMA application, particularly for mining industry, where the required capacities could be highly greater than other industrial fields. On the other hand, the current LiquiCel Extra-Flow modules, having the cross flow with center baffle, offered capacities for scientific and industrial purposes only over 1.7 L/min. This fact limited the use of minor flows, especially in scientific development, affecting the results needed for scaling up. This is relevant for scaling up studies based on experimental work. E.g. our previous work [15], where in order to actually evaluate and compare the GFMA process with others cyanide recovery technologies, the experiment was performed using a LiquiCel Extra-Flow module, and the plant design was based on the Basu correlation (for parallel flow) [17,18]. This wrong assumption underestimated the performance of the GFMA process. Even if the results of this work were promising for the GFMA process with respect to the others technologies, it could have been more conclusive in favor of GFMA.

On the other hand, the selection of the Schoner et al. [51] correlation to simulate the LiquiCel module was based on the analysis of the conditions tested by different authors [51–55]. Table 6 shows the values of the overall mass transfer coefficient obtained from the different mass transfer correlations for the LiquiCel Extra-Flow module proposed. The results of the three first correlations [51–53] were similar, mainly due to the similar experimental conditions used (liquid phase circulating in the shell side, feed flows and Re). Hence, the use of any of these correlations in the simulations performed here would maintain the results obtained. However, the Fouad correlation [54] overestimates the overall mass transfer coefficient due to the Re conditions on the shell side were very low (< 0.1) with respect to the simulated conditions in this work. Finally, the mass transfer correlation from Shen et al. [55] underestimates the value of the overall mass transfer coefficient. Probably because of this correlation, there was an average equation obtained from an analysis of different experimental results, including results from their work (solvent extraction), and gas-liquid extraction systems [56,57]. A semi-empirical correlation for baffled cross-flow modules (LiquiCel modules) was proposed by Sengupta et al. [56] to gas-liquid extraction system, Table 6 where nitrogen gas flowed by lumen side and water circulated on the shell side. Even though, this correlation could be used to estimate mass transfer coefficients of

Table 6
Comparison of overall mass transfer coefficients results from the different mass transfer correlations of the shell side for LiquiCel module, estimated for a feed flow of 2.0 L/min.

Correlation	K, m/s	Experimental system
Schoner et al. [51]	7.36×10^{-5}	Solvent extraction
Baudot et al. [52]	2.0×10^{-5}	Solvent extraction
Zheng et al. [53]	6.70×10^{-5}	Gas absorption
Fouad et al. [54]	2.02×10^{-4}	Solvent extraction
Shen et al. [55]	2.10×10^{-6}	Different systems

baffled cross-flow modules, some empirical parameters required for an estimation have not been reported by the authors (e.g., parameters a and c of the correlation 20 listed in Table 1). Furthermore, the results obtained in the Sengupta study cannot be extrapolated to the cyanide recovery in the GFMA process, due to the operational conditions (Table 1) and extracted compound (oxygen) differ.

4. Conclusions

A performance assessment of different HFMC and mass transfer correlations has been developed for GFMA process to recover cyanide, using a phenomenological model proposed in a previous work. This analysis has demonstrated the relevance of the operational parameters (Re) and module characteristics (type, packing fraction) to select the correct mass transfer correlation between the extensive correlations proposed in the literature. In this context, the correlations by Basu et al. [17,18] and Viegas et al. [37] have the best adjustment with respect to the experimental work for the GFMA process. However, the membrane module assessed in that experimental work was the cylindrical module with parallel flow: a module configuration with no replica for higher capacities for pilot or industrial plants purposes. Furthermore, this type of module presents the worst performance results in terms of the cross flow or fully baffled modules. These issues limit the scaling up and design process for a new application of the GFMA process. This study has compared different modules configurations and their mass transfer correlations proposed in the literature, in order to establish the best configuration modules with perspectives towards the application for design and scaling up. The LiquiCel ExtraFlow module and the fully baffled module proposed by Wang and Cussler have the best performance regarding mass transfer efficiency. Nevertheless, the LiquiCel ExtraFlow modules have no replicas for capacities below 1.7 L/min, limiting experimental or scientific studies for new applications and its further scaling up studies. This limitation can be overcome by developing a new ExtraFlow module for 0.2–1.7 L/min of capacity. On the other hand, the fully baffled module has been developed only for scientific studies with no replicas with high capacity. Likewise, the pressure drop reached in this module has not been reported. A further development of this module focusing on these topics could promote an interesting alternative of industrial modules for the LiquiCel modules, particularly in mining, where the capacities needed are higher than in other industries.

Acknowledgements

The authors gratefully acknowledge the financial support of the National Commission for Scientific and Technological Research (CONICYT Chile) through the Project Fund no. FB0809 PIA CONICYT of Dr. H. Estay and Project FONDECYT 1140208 of Dr. Romero.

References

- [1] M. Imai, S. Furusaki, T. Miyauchi, Separation of volatile materials by gas membranes, *Ind. Eng. Chem. Process Des. Dev.* 21 (1982) 421–426, <http://dx.doi.org/10.1021/i200018a013>.
- [2] Z. Qi, E.L. Cussler, Hollow fiber gas membranes, *AIChE J.* 31 (1985) 1548–1553, <http://dx.doi.org/10.1002/aic.690310918>.
- [3] M. Ulbricht, G. Lakner, J. Lakner, K. Belafi-Bako, TransMembraneChemiSorption of ammonia from sealing water in Hungarian powder metallurgy furnace, *Desalin. Water Treat.* 75 (2017) 253–259, <http://dx.doi.org/10.5004/dwt.2017.20517>.
- [4] A. Hasanoğlu, J. Romero, B. Pérez, A. Plaza, Ammonia removal from wastewater streams through membrane contactors: experimental and theoretical analysis of operation parameters and configuration, *Chem. Eng. J.* 160 (2010) 530–537, <http://dx.doi.org/10.1016/j.cej.2010.03.064>.
- [5] Z. Zhu, Z. Hao, Z. Shen, J. Chen, Modified modeling of the effect of pH and viscosity on the mass transfer in hydrophobic hollow fiber membrane contactors, *J. Memb. Sci.* 250 (2005) 269–276, <http://dx.doi.org/10.1016/j.memsci.2004.10.031>.
- [6] A. Plaza, J. Romero, W. Silva, E. Morales, A. Torres, M.J. Aguirre, Extraction and quantification of SO₂ content in wines using a hollow fiber contactor, *Food Sci. Technol. Int.* 20 (2013) 501–510, <http://dx.doi.org/10.1177/1082013213494900>.
- [7] A. Hasanoğlu, J. Romero, A. Plaza, W. Silva, Gas-filled membrane absorption: a review of three different applications to describe the mass transfer by means of a unified approach, *Desalin. Water Treat.* 51 (2013) 5649–5663, <http://dx.doi.org/10.1080/19443994.2013.769603>.
- [8] C.F. Kenfield, R. Qin, M.J. Semmens, E.L. Cussler, Cyanide recovery across hollow fiber gas membranes, *Environ. Sci. Technol.* 22 (1988) 1151–1155, <http://dx.doi.org/10.1021/es00175a003>.
- [9] A.E. Short, S.F. Haselmann, M.J. Semmens, The GM-IX process: a pilot study for recovering zinc cyanides, *J. Environ. Sci. Heal. Part a-Environ. Sci. Eng. Toxic Hazard. Subst. Control.* 32 (1997) 215–239, <http://dx.doi.org/10.1080/10934529709376537>.
- [10] Z. Shen, B. Han, R. Wickramasinghe, Cyanide removal from wastewater using gas membranes: pilot-scale study, *Water Environ. Res.* 76 (2004) 15–22.
- [11] B. Han, Z. Shen, S.R. Wickramasinghe, Cyanide removal from industrial wastewater using gas membranes, *J. Memb. Sci.* 257 (2005) 171–181, <http://dx.doi.org/10.1016/j.memsci.2004.06.064>.
- [12] Z. Xu, L. Li, Z. Shen, Treatment of praziquantel wastewater using the integrated process of coagulation and gas membrane absorption, *Water Res.* 39 (2005) 2189–2195, <http://dx.doi.org/10.1016/j.watres.2005.04.001>.
- [13] Z. Shen, B. Han, S.R. Wickramasinghe, Cyanide removal from industrial praziquantel wastewater using integrated coagulation-gas-filled membrane absorption, *Desalination* 195 (2006) 40–50, <http://dx.doi.org/10.1016/j.desal.2005.12.008>.
- [14] H. Estay, M. Ortiz, J. Romero, A novel process based on gas filled membrane absorption to recover cyanide in gold mining, *Hydrometallurgy* (2013) 134–135, <http://dx.doi.org/10.1016/j.hydromet.2013.02.012>.
- [15] H. Estay, E. Troncoso, J. Romero, Design and cost estimation of a gas-filled membrane absorption (GFMA) process as alternative for cyanide recovery in gold mining, *J. Memb. Sci.* 466 (2014), <http://dx.doi.org/10.1016/j.memsci.2014.04.045>.
- [16] A. Gabelman, S. Hwang, Hollow fiber membrane contactors, *J. Memb. Sci.* 159 (1999) 61–106, [http://dx.doi.org/10.1016/S0376-7388\(99\)00040-X](http://dx.doi.org/10.1016/S0376-7388(99)00040-X).
- [17] R. Basu, R. Prasad, K.K. Sirkar, Nondispersive membrane solvent back extraction of Phenol, *AIChE J.* 36 (1990) 450–460, <http://dx.doi.org/10.1002/aic.690360314>.
- [18] C.H. Yun, R. Prasad, A.K. Guha, K.K. Sirkar, Hollow fiber solvent extraction removal of toxic heavy metals from aqueous waste streams, *Ind. Eng. Chem. Res.* 32 (1993) 1186–1195, <http://dx.doi.org/10.1021/ie00018a026>.
- [19] M.-C. Yang, E.L. Cussler, Designing hollow-fiber contactors, *AIChE J.* 32 (1986) 1910–1916, <http://dx.doi.org/10.1002/aic.690321117>.
- [20] C.F. Wan, T. Yang, G.G. Lipscomb, D.J. Stookey, T.S. Chung, Design and fabrication of hollow fiber membrane modules, *J. Memb. Sci.* 538 (2017) 96–107, <http://dx.doi.org/10.1016/j.memsci.2017.05.047>.
- [21] S.R. Wickramasinghe, M.J. Semmens, E.L. Cussler, Hollow fiber modules made with hollow fiber fabric, *J. Memb. Sci.* 84 (1993) 1–14, [http://dx.doi.org/10.1016/0376-7388\(93\)85046-Y](http://dx.doi.org/10.1016/0376-7388(93)85046-Y).
- [22] S. Koo, A.S. Sangani, Mass transfer coefficients for laminar longitudinal flow in hollow-fiber contactors, *J. Fluid Mech.* 484 (2003) 255–282, <http://dx.doi.org/10.1017/S0022112003004336>.
- [23] H. Takeuchi, K. Takahashi, M. Nakano, Mass transfer in single oil-containing microporous hollow fiber contactors, *Ind. Eng. Chem. Res.* 29 (1990) 1471–1476, <http://dx.doi.org/10.1021/ie00103a056>.
- [24] W. Zhang, J. Li, G. Chen, W. You, Y. Jiang, W. Sun, Experimental study of mass transfer in membrane absorption process using membranes with different porosities, *Ind. Eng. Chem. Res.* 49 (2010) 6641–6648, <http://dx.doi.org/10.1021/ie1001026>.
- [25] L. Dahuron, E.L. Cussler, Protein extractions with hollow fibers, *AIChE J.* 34 (1988) 130–136, <http://dx.doi.org/10.1002/aic.690340115>.
- [26] R. Prasad, K.K. Sirkar, Dispersion-free solvent extraction with microporous hollow fiber modules, *AIChE J.* 34 (1988) 177–188.
- [27] F. Lipnizki, R.W. Field, Mass transfer performance for hollow fibre modules with shell-side axial feed flow: using an engineering approach to develop a framework, *J. Memb. Sci.* 193 (2001) 195–208, [http://dx.doi.org/10.1016/S0376-7388\(01\)00512-9](http://dx.doi.org/10.1016/S0376-7388(01)00512-9).
- [28] S.R. Wickramasinghe, M.J. Semmens, E.L. Cussler, Mass transfer in various hollow fiber geometries, *J. Memb. Sci.* 69 (1992) 235–250, [http://dx.doi.org/10.1016/0376-7388\(92\)80042-I](http://dx.doi.org/10.1016/0376-7388(92)80042-I).
- [29] M.J. Costello, A.G. Fane, P.A. Hogan, R.W. Schofield, The effect of shell side hydrodynamics on the performance of axial flow hollow fibre modules, *J. Memb. Sci.* 80 (1993) 1–11, [http://dx.doi.org/10.1016/0376-7388\(93\)85127-I](http://dx.doi.org/10.1016/0376-7388(93)85127-I).
- [30] R. Gawroński, B. Wrzesińska, Kinetics of solvent extraction in hollow-fiber contactors, *J. Memb. Sci.* 168 (2000) 213–222, [http://dx.doi.org/10.1016/S0376-7388\(99\)00317-8](http://dx.doi.org/10.1016/S0376-7388(99)00317-8).
- [31] J. Wu, V. Chen, Shell-side mass transfer performance of randomly packed hollow fiber modules, *J. Memb. Sci.* 172 (2000) 59–74, [http://dx.doi.org/10.1016/S0376-7388\(00\)00318-5](http://dx.doi.org/10.1016/S0376-7388(00)00318-5).
- [32] J.-M. Zheng, Z.-K. Xu, J.-M. Li, S.-Y. Wang, Y.-Y. Xu, Influence of random arrangement of hollow fiber membranes on shell side mass transfer performance: a novel model prediction, *J. Memb. Sci.* 236 (2004) 145–151, <http://dx.doi.org/10.1016/j.memsci.2004.02.016>.
- [33] S. Kartohardjono, V. Chen, Mass transfer and fluid hydrodynamics in sealed end hydrophobic hollow fiber membrane gas-liquid contactors, *J. Appl. Membr. Sci. Technol.* 2 (2005) 1–12.
- [34] A.G. Asimakopoulou, A.J. Karabelas, Mass transfer in liquid-liquid membrane-based extraction at small fiber packing fractions, *J. Memb. Sci.* 271 (2006) 151–162, <http://dx.doi.org/10.1016/j.memsci.2005.07.015>.
- [35] A.G. Asimakopoulou, A.J. Karabelas, A study of mass transfer in hollow-fiber membrane contactors – the effect of fiber packing fraction, *J. Memb. Sci.* 282 (2006) 430–441, <http://dx.doi.org/10.1016/j.memsci.2006.05.049>.

- [36] R. Thanedgunbaworn, R. Jiraratananon, M.H. Nguyen, Shell-side mass transfer of hollow fibre modules in osmotic distillation process, *J. Memb. Sci.* 290 (2007) 105–113, <http://dx.doi.org/10.1016/j.memsci.2006.12.021>.
- [37] R.M.C. Viegas, M. Rodriguez, S. Luque, J.R. Alvarez, I.M. Coelho, J.P.S.G. Crespo, Mass transfer correlations in membrane extraction: analysis of Wilson-plot methodology, *J. Memb. Sci.* 145 (1998) 129–142, [http://dx.doi.org/10.1016/S0376-7388\(98\)00074-X](http://dx.doi.org/10.1016/S0376-7388(98)00074-X).
- [38] J.-M. Zheng, Y.-Y. Xu, Z.-K. Xu, Shell side mass transfer characteristics in a parallel flow hollow fiber membrane module, *Sep. Sci. Technol.* 38 (2003) 1247–1267, <http://dx.doi.org/10.1081/SS-120018808>.
- [39] J.J. Cai, K. Hawboldt, M.A. Abdi, Analysis of the effect of module design on gas absorption in cross flow hollow membrane contactors via computational fluid dynamics (CFD) analysis, *J. Memb. Sci.* 520 (2016) 415–424, <http://dx.doi.org/10.1016/j.memsci.2016.07.054>.
- [40] X. Yu, L. An, J. Yang, S.-T. Tu, J. Yan, CO₂ capture using a superhydrophobic ceramic membrane contactor, *J. Memb. Sci.* 496 (2015) 1–12, <http://dx.doi.org/10.1016/j.memsci.2015.08.062>.
- [41] W. Rongwong, C. Fan, Z. Liang, Z. Rui, R.O. Idem, P. Tontiwachwuthikul, Investigation of the effects of operating parameters on the local mass transfer coefficient and membrane wetting in a membrane gas absorption process, *J. Memb. Sci.* 490 (2015) 236–246, <http://dx.doi.org/10.1016/j.memsci.2015.04.071>.
- [42] X. Wang, J. Gao, J. Zhang, X. Zhang, R. Guo, Theoretical and experimental studies on acetylene absorption in a polytetrafluoroethylene hollow-fiber membrane contactor, *Chem. Eng. Technol.* 38 (2015) 215–222, <http://dx.doi.org/10.1002/ceat.201400338>.
- [43] D. Albarracin Zaidiza, J. Billaud, B. Belaissaoui, S. Rode, D. Roizard, E. Favre, Modeling of CO₂ post-combustion capture using membrane contactors, comparison between one- and two-dimensional approaches, *J. Memb. Sci.* 455 (2014) 64–74, <http://dx.doi.org/10.1016/j.memsci.2013.12.012>.
- [44] S. Boributh, W. Rongwong, S. Assabumrungrat, N. Laosiripojana, R. Jiraratananon, Mathematical modeling and cascade design of hollow fiber membrane contactor for CO₂ absorption by monoethanolamine, *J. Memb. Sci.* 401–402 (2012) 175–189, <http://dx.doi.org/10.1016/j.memsci.2012.01.048>.
- [45] S. Bocquet, A. Torres, J. Sanchez, G.M. Rios, J. Romero, Modeling the mass transfer in solvent-extraction processes with hollow-fiber membranes, *AIChE J.* 51 (2005) 1067–1079, <http://dx.doi.org/10.1002/aic.10461>.
- [46] B. Cancino-Madariaga, R. Ruby, C. Astudillo Castro, J. Saavedra Torrico, M. Lutz Riquelme, Analysis of the membrane fouling mechanisms involved in clarified grape juice ultrafiltration using statistical tools, *Ind. Eng. Chem. Res.* 51 (2012) 4017–4024, <http://dx.doi.org/10.1021/ie201921x>.
- [47] T.P. Ryan, *Mod. Eng. Stat.* (2006), <http://dx.doi.org/10.1002/9780470128442>.
- [48] K.L. Wang, E.L. Cussler, Baffled membrane modules made with hollow fiber fabric, *J. Memb. Sci.* 85 (1993) 265–278, [http://dx.doi.org/10.1016/0376-7388\(93\)85280-A](http://dx.doi.org/10.1016/0376-7388(93)85280-A).
- [49] P.H.M. Feron, A.E. Jansen, CO₂ separation with polyolefin membrane contactors and dedicated absorption liquids: performances and prospects, *Sep. Purif. Technol.* 27 (2002) 231–242, [http://dx.doi.org/10.1016/S1383-5866\(01\)00207-6](http://dx.doi.org/10.1016/S1383-5866(01)00207-6).
- [50] D. Bhaumik, S. Majumdar, K.K. Sirkar, Absorption of CO₂ in a transverse flow hollow fiber membrane module having a few wraps of the fiber mat, *J. Memb. Sci.* 138 (1998) 77–82, [http://dx.doi.org/10.1016/S0376-7388\(97\)00208-1](http://dx.doi.org/10.1016/S0376-7388(97)00208-1).
- [51] P. Schoner, P. Plucinski, W. Nitsch, U. Daiminger, Mass transfer in the shell side of cross flow hollow fiber modules, *Chem. Eng. Sci.* 53 (1998) 2319–2326, [http://dx.doi.org/10.1016/S0009-2509\(98\)00097-9](http://dx.doi.org/10.1016/S0009-2509(98)00097-9).
- [52] A. Baudot, J. Flourey, H.E. Smorenburg, Liquid-liquid extraction of aroma compounds with hollow fiber contactor, *AIChE J.* 47 (2001) 1780–1793, <http://dx.doi.org/10.1002/aic.690470810>.
- [53] J.M. Zheng, Z.W. Dai, F.S. Wong, Z.K. Xu, Shell side mass transfer in a transverse flow hollow fiber membrane contactor, *J. Memb. Sci.* 261 (2005) 114–120, <http://dx.doi.org/10.1016/j.memsci.2005.02.035>.
- [54] E.A. Fouad, H.J. Bart, Separation of zinc by a non-dispersion solvent extraction process in a hollow fiber contactor, *Solvent Extr. Ion. Exch.* 25 (2007) 857–877, <http://dx.doi.org/10.1080/07366290701634610>.
- [55] S. Shen, S.E. Kentish, G.W. Stevens, Solvent extraction and ion exchange shell-side mass-transfer performance in hollow-fiber membrane contactors, *Solvent Extr. Ion. Exch.* 28 (2010) 817–844, <http://dx.doi.org/10.1080/07366299.2010.515176>.
- [56] A. Sengupta, P.A. Peterson, B.D. Miller, J. Schneider, C.W. Fulk, Large-scale application of membrane contactors for gas transfer from or to ultrapure water, *Sep. Purif. Technol.* 14 (1998) 189–200, [http://dx.doi.org/10.1016/S1383-5866\(98\)00074-4](http://dx.doi.org/10.1016/S1383-5866(98)00074-4).
- [57] S.A. Tarafder, C.I. McDermott, C. Schüth, Vacuum assisted removal of volatile to semi volatile organic contaminants from water using hollow fiber membrane contactors. II: a hybrid numerical-analytical modeling approach, *J. Memb. Sci.* 292 (2007) 9–16, <http://dx.doi.org/10.1016/j.memsci.2007.01.002>.
- [58] D.W. Johnson, M.J. Semmens, J.S. Gulliver, Diffusive transport across unconfined hollow fiber membranes, *J. Memb. Sci.* 128 (1997) 67–81.
- [59] L. Bao, G.G. Lipscomb, Entry mass transfer in axial flows through randomly packed fiber bundles, *AIChE J.* 45 (1999) 2346–2356, <http://dx.doi.org/10.1002/aic.690451110>.